

Nonequilibrium density of states and distribution functions for strongly correlated materials across the Mott transition

J. K. Freericks and A. V. Joura

Department of Physics, Georgetown University, Washington, DC 20057, U.S.A.

Abstract. We examine the local density of states and the momentum-dependent distribution functions as they evolve in time for systems described by the Falicov-Kimball model initially in equilibrium, and then driven by a large uniform electric field turned on at time $t = 0$. We use exact dynamical mean-field theory, extended to nonequilibrium situations, to solve the problem. We focus on the accuracy of the numerics and on the interesting new features brought about by the strong correlations.

1.1 Introduction

There has been increasing interest in the behavior of quantum mechanical systems that are driven out of equilibrium due to the presence of large external electrical fields, motivated in part by the miniaturization of electronics and nanotechnology, which routinely have large electric fields placed over structures with small feature sizes. The general formalism for the nonequilibrium many-body problem was worked out by Kadanoff and Baym [Kadanoff and Baym1962] and by Keldysh [Keldysh1964] in the 1960s. Unfortunately, at that time there was no known way to solve the resulting equations in cases with strong electron correlations, and most analysis was based on perturbative approaches in the interaction strength (because the noninteracting Green's functions in a field were known exactly [Jauho and Wilkins1984], the theory treated all electric field effects to all orders in the field). In 1989, dynamical mean-field theory was invented [Brandt and Mielsch1989], and it has allowed us to solve nearly all equilibrium many-body problems in solid-state physics [Georges et al.1996]. It has recently been generalized to the nonequilibrium case [Freericks et al.2006b, Freericks2007, Freericks et al.2006a, Freericks et al.2007, Turkowski and Freericks2007], and the work we report on here describes some of the results emerging from these calculations.

The model Hamiltonian we will consider is the Falicov-Kimball model [Falicov and Kimball1969], which involves two sets of spinless electrons—conduction

electrons (which hop between neighboring lattice sites and are denoted by c) and localized electrons (which do not hop and are denoted by f). The two electrons have a mutual on-site Coulomb repulsion of strength U when two electrons are in the same unit cell. The Hamiltonian (in the absence of an external field) is

$$\mathcal{H} = -\frac{t^*}{2\sqrt{d}} \sum_{\langle ij \rangle} (c_i^\dagger c_j + c_j^\dagger c_i) + U \sum_i c_i^\dagger c_i f_i^\dagger f_i, \quad (1.1)$$

where the creation and annihilation operators satisfy the usual fermionic anticommutation relations. This model is the simplest many-body problem that has a Mott-like metal-insulator transition when the conduction and localized electrons are both half-filled. We work on a hypercubic lattice in infinite-dimensions [Metzner and Vollhardt1989], where the noninteracting density of states is $\rho(\epsilon) = \exp(-\epsilon^2)/\sqrt{\pi}$; we use the hopping energy t^* as the energy unit.

1.2 Formalism

We initially prepare the system in an equilibrium state with a temperature $1/\beta = 0.1$ and turn on a uniform electric field at $t = 0$ (we neglect the transient magnetic field present only at times close to $t = 0$). The uniform electric field is described by a uniform vector potential in the Hamiltonian gauge [$A = -Et\theta(t)$]. We are interested in finding the local many-body density of states (DOS) as a function of time, which is the double-time expectation value $\langle \{c_i^\dagger(t)c_i(t') + c_i(t')c_i^\dagger(t)\} \rangle$ and in finding the distribution of electrons in momentum space as a function of time, which is the equal time expectation value $\langle c_{\mathbf{k}}^\dagger(t)c_{\mathbf{k}}(t) \rangle$ that measures how the electrons are distributed over the Brillouin zone. The DOS is normally described as a function of average time $T = (t + t')/2$ and of frequency ω , after Fourier transforming the time-dependent expectation value over the relative time $t_{rel} = t - t'$.

Both the DOS and the distribution functions can be found from the so-called contour-ordered Green's function $G_{ij}(t, t')$

$$G_{ij}(t, t') = -i \text{Tre}^{-\beta\mathcal{H}(t=-5)} \mathcal{T}_c c_i(t) c_j^\dagger(t') / \mathcal{Z}, \quad (1.2)$$

where each time argument t and t' lies on the Kadanoff-Baym-Keldysh contour, depicted in Fig. 1.1 for the problems we will be analyzing (the field is described by the spatially uniform vector potential A). The time-dependence of the operators is in the Heisenberg representation, the time-ordering operator \mathcal{T}_c orders times along the contour, and $\mathcal{Z} = \text{Tre}^{-\beta\mathcal{H}(t=-5)}$ is the equilibrium partition function (which could be evaluated at *any* time prior to the time the field turns on because the Hamiltonian is time-independent in equilibrium). The Green's functions defined on this contour have a 3×3 matrix structure

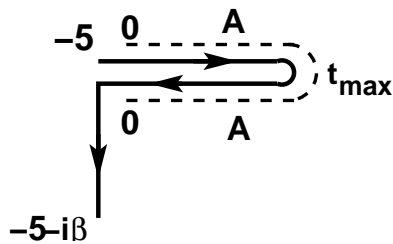


Fig. 1.1. Kadanoff-Baym-Keldysh contour for calculating nonequilibrium Green's functions. The initial 5 units of time are needed to ensure the system properly represents the equilibrium solution, while the field is turned on at $t = 0$ as represented by the nonzero vector potential A running out to t_{max} . The contour then continues to run back to $t = -5$ and then down the imaginary axis a distance β .

to them as described by Wagner [Wagner1991]; this is needed to determine the transient response effects we are interested in.

The DOS is found from the local limit ($i = j$) of the real-space retarded Green's function

$$G_{ij}^R(t, t') = -i \text{Tr} e^{-\beta \mathcal{H}(t=-5)} \{c_i(t) c_j^\dagger(t') + c_j^\dagger(t') c_i(t)\} / \mathcal{Z}, \quad (1.3)$$

while the distribution function is found from the equal-time limit of the so-called momentum-dependent lesser Green's function

$$G_{\mathbf{k}}^<(t, t') = i \text{Tr} e^{-\beta \mathcal{H}} c_{\mathbf{k}}^\dagger(t') c_{\mathbf{k}}(t) / \mathcal{Z}, \quad (1.4)$$

expressed in terms of momentum-dependent creation and annihilation operators. Both of these quantities can be directly extracted from the contour-ordered Green's function.

The vector potential is introduced into the Hamiltonian via the Peierls substitution [Peierls1933], and it modifies the kinetic energy operator

$$-\frac{t^*}{2\sqrt{d}} \sum_{\langle ij \rangle} (c_i^\dagger c_j + c_j^\dagger c_i) = \sum_{\mathbf{k}} \epsilon_{\mathbf{k}} c_{\mathbf{k}}^\dagger c_{\mathbf{k}} \rightarrow \sum_{\mathbf{k}} \epsilon_{\mathbf{k}-\mathbf{A}(t)} c_{\mathbf{k}}^\dagger c_{\mathbf{k}}, \quad (1.5)$$

where we have made a Fourier transformation, and $\epsilon_{\mathbf{k}} = -t^* \sum_i \cos \mathbf{k}_i / \sqrt{d}$ is the bandstructure for nearest-neighbor hopping on a hypercubic lattice [Metzner and Vollhardt1989].

Because the noninteracting Hamiltonian commutes with itself at different times, the exact noninteracting Green's functions in a field are easy to determine, and form the starting point for solving the nonequilibrium problem [Turkowski and Freericks2005]. The noninteracting contour-ordered Green's function in a field satisfies

$$\begin{aligned} G_{\mathbf{k}}^{\text{non}}(t, t') &= i\theta_c(t, t') \exp \left[-i \int_{t'}^t d\bar{t} \{ \epsilon_{\mathbf{k}-\mathbf{A}(\bar{t})} - \mu \} \right] [1 - f(\epsilon_{\mathbf{k}} - \mu)] \\ &\quad - i\theta_c(t', t) \exp \left[-i \int_{t'}^t d\bar{t} \{ \epsilon_{\mathbf{k}-\mathbf{A}(\bar{t})} - \mu \} \right] f(\epsilon_{\mathbf{k}} - \mu), \end{aligned} \quad (1.6)$$

where the theta function $\theta_c(t, t')$ is equal to one if t is farther along the contour than t' (and is equal to zero otherwise), the integral in the exponential function runs along the contour from t' to t (note that $\mathbf{A}(t) = 0$ on the imaginary axis and for real times less than zero), and $f(x) = 1/[1 + \exp(\beta x)]$ is the Fermi-Dirac distribution function.

It turns out that the momentum-dependent Green's function depends on only two scalar quantities when the electric field lies in the diagonal (1,1,1,...) direction: the band structure $\epsilon_{\mathbf{k}}$ and a second bandstructure $\bar{\epsilon}_{\mathbf{k}} = -t^* \sum_i \sin \mathbf{k}_i / \sqrt{d}$. The local Green's function can be found by summing the momentum-dependent Green's function over all momentum, which can be replaced by a two-dimensional integral over ϵ and $\bar{\epsilon}$ weighted by the joint density of states which is equal to $\rho(\epsilon)\rho(\bar{\epsilon})$ [Turkowski and Freericks2005]. All of the Green's functions and self-energies are described by two-time continuous matrix operators, which are discretized into general complex matrices when we perform numerical calculations (because it is a nonequilibrium problem with both a transient and steady-state response, we work in a time formalism). We vary the discretization size along the real time axis, but keep the discretization along the imaginary axis fixed at a size of $\Delta\tau = 0.1$ (100 points for $1/\beta = 0.1$). The initial 5 units of time are sufficient to allow the system to accurately display its equilibrium properties prior to the field being turned on at $t = 0$. For most calculations presented here, we use $t_{\max} = 35$. The matrices have sizes ranging from 900×900 ($\Delta t = 0.1$ when $t_{\max} = 35$) up to 4100×4100 ($\Delta t = 0.02$ when $t_{\max} = 35$). The local Green's function is then calculated by evaluating a two-dimensional Gaussian integral of a matrix valued integrand that requires one matrix inversion and two matrix multiplications to calculate. This is the most time-consuming part of the computation.

The nonequilibrium dynamical mean-field theory algorithm is then essentially the same as the equilibrium one [Freericks et al.2006b, Freericks2007, Freericks et al.2006a, Turkowski and Freericks2007] (all Green's functions and self-energies are dense general complex matrices): (i) begin with a guess for the self-energy (we use the equilibrium self-energy expressed in a time representation); (ii) calculate the local Green's function from the self-energy by using a two-dimensional matrix-valued quadrature {the integrand is $[1 - G^{non}(\epsilon_{\mathbf{k}}, \bar{\epsilon}_{\mathbf{k}})\Sigma]^{-1}G^{non}(\epsilon_{\mathbf{k}}, \bar{\epsilon}_{\mathbf{k}})$, where G^{non} is the exact noninteracting Green's function on the lattice in the electric field [see Eq. (1.6)]; (iii) extract the dynamical mean field λ by removing the self-energy from the local Green's function [$\lambda = -G^{-1} - \Sigma + G_{imp}^{non}(\mu)$, with $G_{imp}^{non}(\mu)$ the *free impurity* Green's function with a chemical potential μ and given by Eq. (1.6) with both $\epsilon_{\mathbf{k}} = 0$ and $\mathbf{A} = 0$]; (iv) solve the impurity problem in the time-dependent dynamical mean field for the new Green's function $\{G = (1 - w_1)[G_{imp}^{non}(\mu)^{-1} - \lambda]^{-1} + w_1[G_{imp}^{non}(\mu - U)^{-1} - \lambda]^{-1}$, where $w_1 = 1/2$ is the density of the localized electrons}; (v) extract the new self-energy from Dyson's equation [$\Sigma = G_{imp}^{non}(\mu)^{-1} - \lambda - G^{-1}$] and proceed to step (ii) until fully converged.

The nonequilibrium algorithm parallelizes [Freericks et al.2006b, Freericks2007, Freericks et al.2007] in the master-slave approach—the master sends

the self-energies to each slave node, which calculates and accumulates the integrands for each quadrature point and then forwards the accumulated results to the master. The master then calculates the impurity part of the algorithm [steps (iii)–(v)], checks the convergence and repeats if necessary. Using BLAS and LAPACK routines makes for a highly efficient algorithm which has achieved over 65% of peak speed on 2032 cores of a SGI Altix supercomputer [Freericks et al.2007].

In addition to the transient nonequilibrium algorithm described above, one can also examine steady-state properties. At the moment, the formalism has only been developed for the retarded Green's function, and hence for the local DOS. Future work will develop techniques for the lesser Green's function. In a steady-state formalism, we imagine the system has been prepared at a time $-t_1$ in an equilibrium state, and then at time $-t_2$ (with $-t_1 < -t_2$), an electric field is turned on. We then take the limit where $-t_1 \rightarrow -\infty$ and $-t_2 \rightarrow -\infty$ while maintaining $-t_1 < -t_2$, and examine the Green's functions a long time after the field was turned on. In this case, because all memory of the equilibrium state is lost as we moved into the steady-state response, we can examine the retarded Green's function directly in real time, and do not need to consider the three-part Kadanoff-Baym-Keldysh contour (this statement may not seem to obviously hold, but we will see how the steady-state DOS emerging from this result does appear to be the limit of the transient DOS for large average times).

The starting point is the Dyson equation for the retarded Green's function in real time, which satisfies

$$G_{\mathbf{k}}^R(t, t') = G_{\mathbf{k}}^{R,non}(t, t') + \int d\bar{t} \int d\bar{t}' G_{\mathbf{k}}^{R,non}(t, \bar{t}) \Sigma(\bar{t}, \bar{t}') G_{\mathbf{k}}^R(\bar{t}', t'), \quad (1.7)$$

with the noninteracting retarded Green's function given by [Turkowski and Freericks2007]

$$\begin{aligned} G_{\mathbf{k}}^{R,non}(t, t') &= -i\theta(t - t') \exp \left[-i \int_{t'}^t d\bar{t} (\epsilon_{\mathbf{k}+E\bar{t}} - \mu) \right] \\ &= -i\theta(t_{rel}) \exp \left[-i \frac{2(\epsilon_{\mathbf{k}} \cos ET - \bar{\epsilon}_{\mathbf{k}} \sin ET)}{E} \sin \frac{Et_{rel}}{2} + i\mu t_{rel} \right], \end{aligned} \quad (1.8)$$

where we used $\mathbf{A}(t) = -\mathbf{E}t$ because the field was turned on in the infinite past. The noninteracting Green's function satisfies two important identities. The first we call the *gauge property*, and is

$$G_{\mathbf{k}+E\bar{t}}^{R,non}(t, t') = G_{\mathbf{k}}^{R,non}(t + \bar{t}, t' + \bar{t}) = G_{\mathbf{k}}^{R,non}(T + \bar{t}, t_{rel}), \quad (1.9)$$

where the second equality expresses the Green's function in the Wigner coordinates of average and relative time. The second is the *Bloch periodicity property*

$$\begin{aligned} G_{\mathbf{k}}^{R,non}(t + t_{Bloch}, t' + t_{Bloch}) &= G_{\mathbf{k}}^{R,non}(t, t') \\ G_{\mathbf{k}}^{R,non}(T + t_{Bloch}, t_{rel}) &= G_{\mathbf{k}}^{R,non}(T, t_{rel}), \end{aligned} \quad (1.10)$$

where $t_{Bloch} = 2\pi/E$ is the Bloch period.

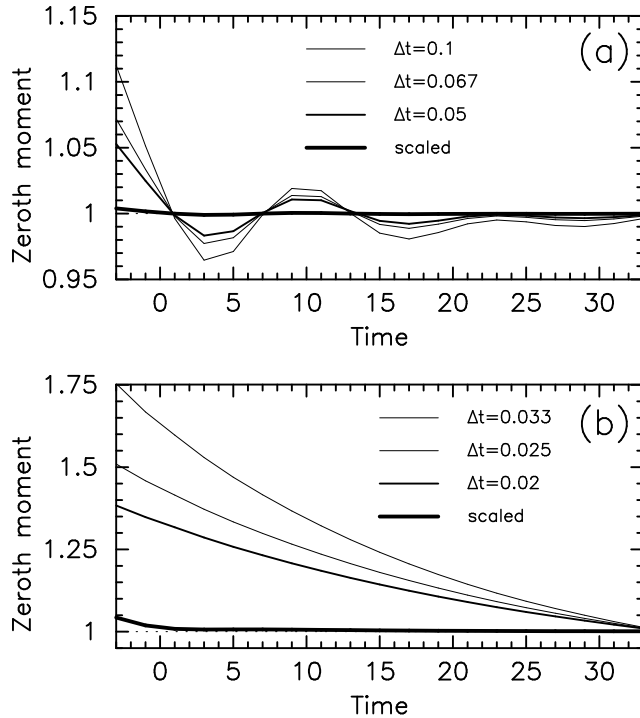


Fig. 1.2. Zeroth moment of the local DOS as a function of average time for the case (a) $U = 0.5$ (strongly scattering metal) and (b) $U = 2$ (moderate gap Mott insulator). We plot results for specific discretizations of the Kadanoff-Baym-Keldysh contour, and for results extrapolated to zero discretization. The extrapolated results are quite accurate, but the accuracy worsens as U increases, and in the equilibrium phase before the field is turned on (the dotted line is the exact result).

The next step is to make an assumption that the local retarded self-energy is independent of average time. This can be seen to hold from an iterative argument as follows—start with the self-energy equal to zero (which obviously is independent of average time). Then the local Green’s function is independent of average time because it is equal to the noninteracting Green’s function and the average time dependence for the local noninteracting Green’s function vanishes due to the gauge property. Hence the dynamical mean-field will be average-time independent and so will the impurity Green’s function and self-energy. Continuing the DMFT iterations will not introduce any average time dependence, so the final converged self-energy will be independent of average time. One can ask whether there could also be a solution where the self-energy depends on average time; we checked this with the transient formalism, and

find that as we approach the steady state the self-energy changes more slowly for long times indicating it is becoming average-time independent. While not a proof, this is a strong argument in favor of the initial assumption that we make. If the retarded self-energy is average-time independent, then one can show from the Dyson equation that the momentum-dependent Green's function satisfies both the Bloch periodicity property and the gauge property and hence that the local retarded Green's function is independent of average time. Thus, we have motivated the assumption that the local retarded self-energy and the local interacting retarded Green's function are independent of average time and the momentum-dependent interacting retarded Green's function satisfies both the gauge property and the Bloch periodicity property. This implies that we can perform a Fourier transformation with respect to the relative time, and a discrete Fourier series expansion with respect to the average time, with the only frequencies appearing being the Bloch frequencies $\nu_n = nE$

$$G_{\mathbf{k}}^R(T, t_{rel}) = \frac{1}{2\pi} \sum_n \int d\omega G_{\mathbf{k}}^R(\nu_n, \omega) e^{-i\nu_n T - i\omega t_{rel}}, \quad (1.11)$$

and similar expansions for the noninteracting Green's function and the self-energy (note that most researchers assume a much stronger result, that the steady state is independent of average time *by definition*, but there does not appear to be any proof of this on a lattice, and indeed, the lesser Green's functions for the noninteracting system and the momentum-dependent Green's functions for the interacting system *do not* satisfy such an assumption, but they do satisfy the Bloch periodicity property). Using this representation, the Dyson equation becomes

$$G_{\mathbf{k}}^R(\nu_n, \omega) = G_{\mathbf{k}}^{R,non}(\nu_n, \omega) + \sum_m G_{\mathbf{k}}^{R,non}(\nu_m, \omega + \frac{1}{2}\nu_n - \frac{1}{2}\nu_m) \times \Sigma(\omega + \frac{1}{2}\nu_n - \nu_m) G_{\mathbf{k}}^R(\nu_n - \nu_m, \omega - \frac{1}{2}\nu_m), \quad (1.12)$$

which has an underlying matrix structure to it that allows us to solve for the $G_{\mathbf{k}}^R(\nu_n, \omega + \frac{1}{2}\nu_m)$ for all m and n (with ω fixed); note that the self-energy is independent of the Bloch frequency because it has no average time dependence. When we solve for the DOS, we need only solve in a frequency range from $0 \leq \omega < E$, because all frequencies outside of that range are coupled together and automatically determined when we solve the Dyson equation. The local Green's function (and hence the local DOS) is found by summing the momentum-dependent Green's function over all momentum, which requires a two-dimensional Gaussian integration (but of a scalar quantity now, rather than a matrix). Because we sum over all momentum, the gauge property tells us the local DOS is independent of average time, and hence we need to evaluate the $\nu_n = 0$ component only

$$\rho^{DOS}(\omega) = -\frac{1}{\pi} \text{Im} \sum_{\mathbf{k}} G_{\mathbf{k}}^R(\nu_n = 0, \omega). \quad (1.13)$$

Note that the steady-state DOS for the Falicov-Kimball model turns out to have no temperature dependence, just like the equilibrium DOS [van Dongen1992]. In our case, the proof is direct, because the temperature never enters the equations that are employed to solve for the retarded Green's function.

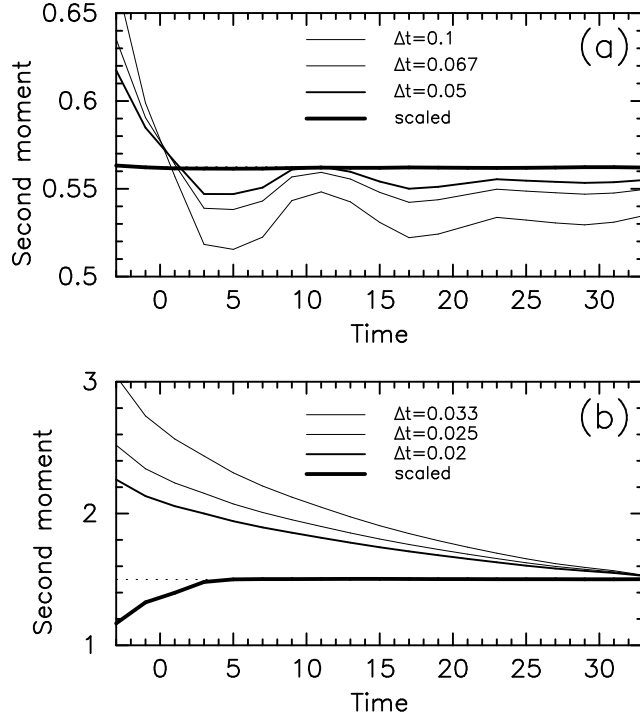


Fig. 1.3. Second moment of the local DOS as a function of average time for the case (a) $U = 0.5$ (strongly scattering metal) and (b) $U = 2$ (moderate gap Mott insulator). We plot results for specific discretizations of the Kadanoff-Baym-Keldysh contour, and for results extrapolated to zero discretization. The dotted line is the exact result.

1.3 Results

We start by calculating the local DOS for the nonequilibrium system. We will be examining systems described by the Falicov-Kimball model at half filling for the conduction electrons and the localized electrons. The system starts in equilibrium with $1/\beta = 0.1$ and has the field turned on at $t = 0$. The field is directed along the diagonal of the infinite-dimensional hypercube and the magnitude of each Cartesian component is equal to $E = 0.5$. We will

plot the DOS as a function of frequency for different average times. But first, we want to verify the accuracy of the calculations, since we have discretized the Kadanoff-Baym-Keldysh contour. This is accomplished by examining sum rules for the DOS [White1991, Turkowski and Freericks2006]. The sum rules examine moments of the local DOS which can be related to the equal time Green's function and its derivatives with respect to the relative time. Since the DOS is determined by the retarded Green's function, we examine the sum rules for the retarded Green's function which turn out to be independent of the electric field. In particular, the zeroth moment sum rule is equal to 1 and the second moment sum rule is equal to $0.5 + U^2/4$. Each of these moments can be directly calculated numerically from the contour-ordered Green's functions. In general, we find the results for a given discretization have errors, which can become quite large, but when we extrapolate the results to zero discretization size (usually with a quadratic Lagrange interpolation formula), we find that agreement is better than 1% for $U = 0.5$ and better than 5% for $U = 2$.

The accuracy for the second moment is not as precise, as one might expect because it is more difficult to accurately determine (see Fig. 1.3). The metallic case still has high accuracy (errors less than 1% for the extrapolated result), but the Mott insulator has much reduced accuracy (less than 30% error for the extrapolated result). But if we examine these results more carefully, we see that the largest deviation occurs at early times, in the equilibrium state. Indeed, the system actually improves the accuracy rather dramatically when it is in nonequilibrium, and the overall error is only a few percent for times larger than 5 units after the field is turned on. This is typically what we see with much of our data, where the real-time formalism is less accurate for equilibrium results than it is for nonequilibrium results.

Having established that we can achieve highly accurate solutions by scaling our data, we next move to examining the local DOS as a function of average time for the metal and the Mott insulator. We continue to scale our data to the zero discretization limit so we can achieve high accuracy (we use $\Delta t = 0.1, 0.067,$ and 0.05 for $U = 0.5$ and $\Delta t = 0.033, 0.025,$ and 0.02 for $U = 2$). In Fig. 1.4, we plot the DOS for a few different values of average time when $U = 0.5$. Panel (a) is a near equilibrium result (the field is turned on at $T = 0$). As the average time increases, the system first appears to develop broadened peaks at the Bloch frequencies $n/2$; those peaks then evolve into a series of minibands with more complex structure by the steady-state limit. Note that we used the transient nonequilibrium DMFT algorithm for all finite times, and the completely different steady-state nonequilibrium DMFT algorithm for the last panel. The similarity of this data clearly indicates that the transient results are approaching the steady-state results. Note further that a close examination of the $T = 23$ data shows that it appears to deviate more from the steady state than the $T = 17$ data. This is most likely an artefact of the truncation of the range of t_{rel} values that are calculated at that average time. We lose precision for the Fourier transform as we approach the maximal time on the Kadanoff-Baym-Keldysh contour because the range of t_{rel} for which

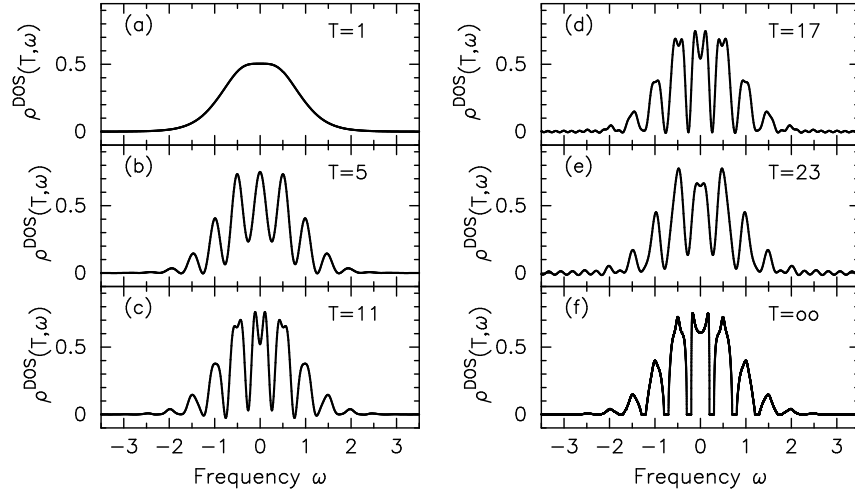


Fig. 1.4. Local DOS as a function of average time for $U = 0.5$ and $E = 0.5$. Note how the system evolves from a near equilibrium DOS to the nonequilibrium steady state.

we have data shrinks to zero at the maximal T value. Hence the detailed structure in the DOS becomes hard to represent with the range of relative time values that we have (especially the fine structure present in the peaks).

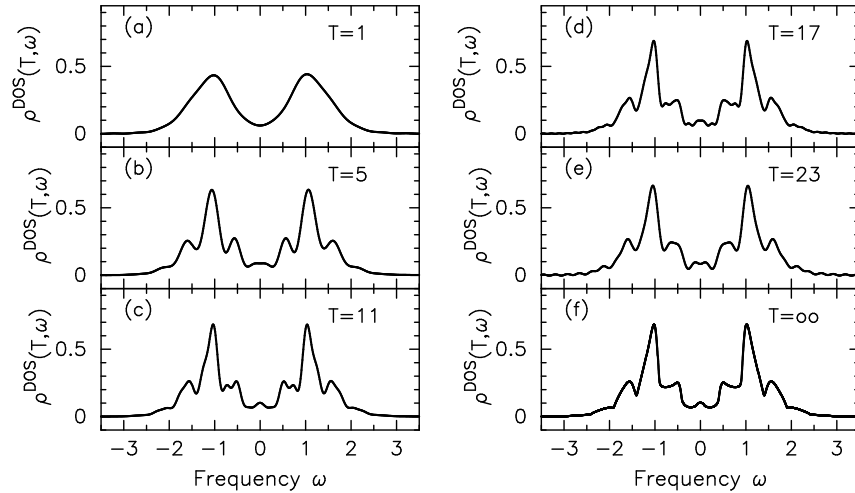


Fig. 1.5. Local DOS as a function of average time for $U = 2$ and $E = 0.5$. Note how the system evolves from a near equilibrium DOS to the nonequilibrium steady state.

In Fig. 1.5, we show a similar plot, but now for the Mott insulator with $U = 2$ (by this we mean the system has undergone the Mott transition in equilibrium; on a hypercubic lattice no true gap develops, because the DOS vanishes only at one point in frequency which might more correctly be called a pseudogap, but there is still a wide region, reminiscent of a Mott gap, where the DOS is exponentially small around this point where the DOS vanishes). The field creates a number of additional peaks in the DOS, but does not have actual minibands form, as the minibands now all overlap with one another. The peak structures are all concentrated near the Bloch frequencies, and there is a small peak that develops at $\omega = 0$ in the steady state. This implies that the driving of the system by the electric field creates “subgap states” that have a metallic character to the DOS! This is because the energy pumped into the system by the field is sufficient to overcome the Mott gap formation.

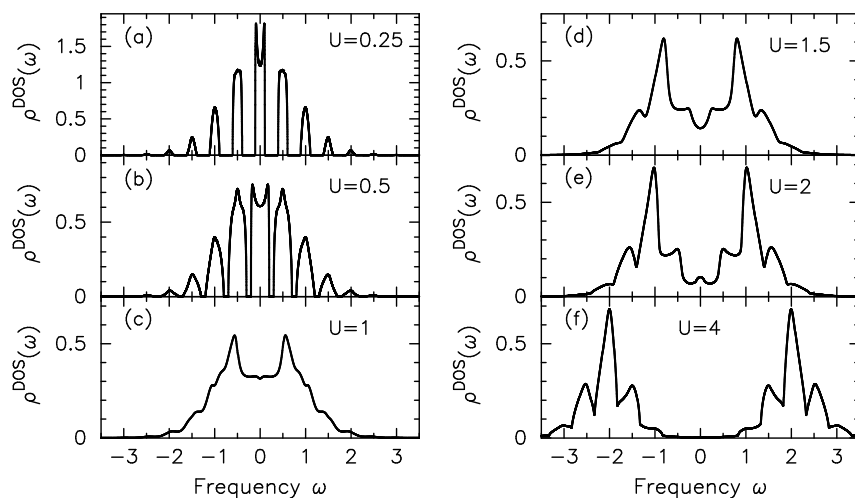


Fig. 1.6. Local DOS in the steady state for $U = 0.25, 0.5, 1, 1.5, 2,$ and 4 with $E = 0.5$. Note how the system evolves from a broadened Wannier-Stark ladder to a “perturbed” Mott insulator with upper and lower Hubbard bands.

In Fig. 1.6, we plot the steady-state DOS in a field (of strength $E = 0.5$) for different values of U . When $U = 0$, the steady state DOS is the Wannier-Stark ladder of delta functions located at the Bloch frequencies, and weighted by a DOS factor. As scattering is turned on, we expect the delta functions to broaden. Indeed, we see this in panel (a), for $U = 0.25$, except the delta function at $\omega = 0$ is broadened with a double-peak structure, separated by U . As U increases further in the metal [panels (b) and (c)], the splitting of the “zeroth” miniband continues to increase, but all of the bands broaden and then eventually merge into a complicated DOS by the time $U = 1$. As U increases further into the Mott insulator, the main peak continues to split, and

the DOS develops the upper and lower Hubbard bands, with an additional “corrugation” induced by the field. Surprisingly, for $U = 2$, the DOS develops a small metal-like peak around $\omega = 0$.

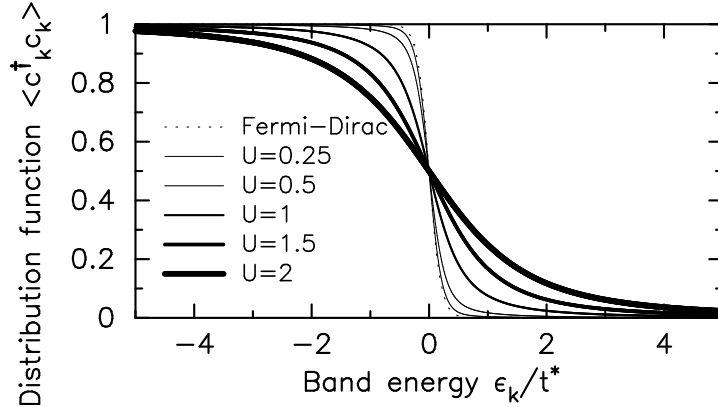


Fig. 1.7. Equilibrium distribution function $\langle c_{\mathbf{k}}^\dagger c_{\mathbf{k}} \rangle = -iG^<(\epsilon_{\mathbf{k}}, t, t)$ for the Falicov-Kimball model at half filling and different U values (the metal-insulator transition takes place at $U = \sqrt{2}$). This data is for $1/\beta = 0.1$.

Next, we focus on calculating the distribution functions in momentum space as they evolve from the equilibrium distribution to the nonequilibrium steady state. But to start, we first want to show the equilibrium distribution functions for different interaction strengths at $1/\beta = 0.1$. This is plotted in Fig. 1.7. The equilibrium distribution function depends only on $\epsilon_{\mathbf{k}}$, and becomes the Fermi-Dirac distribution $1/[1 + \exp(\beta\epsilon_{\mathbf{k}})]$ as $U \rightarrow 0$ (dashed line). As the scattering increases, the distribution function deviates more and more from the noninteracting result (the Mott insulator transition occurs at $U = \sqrt{2}$ in this model).

In nonequilibrium, the distribution function depends on two band energies $\epsilon_{\mathbf{k}}$ and $\bar{\epsilon}_{\mathbf{k}}$, so it is more complicated to present the results (for this work we show results for the Green’s functions in the Hamiltonian gauge rather than making the transformation to gauge-invariant Green’s functions—for this field, the transformation [Bertoncini and Jauho1991, Turkowski and Freericks2007] involves just a rotation in the $\epsilon - \bar{\epsilon}$ plane). We will show the behavior for some specific values of $\epsilon_{\mathbf{k}}$ and $\bar{\epsilon}_{\mathbf{k}}$. There is one technical detail we use for calculating the distribution functions. In this formalism, we can find both the retarded and the lesser Green’s functions at equal times. The retarded Green’s functions should have a value of 1 everywhere because they are equal to the equal time anticommutator of the creation and annihilation operators. But for a given discretization, we often find that the retarded Green’s function does not equal one at equal times (see Fig. 1.2). Hence, we

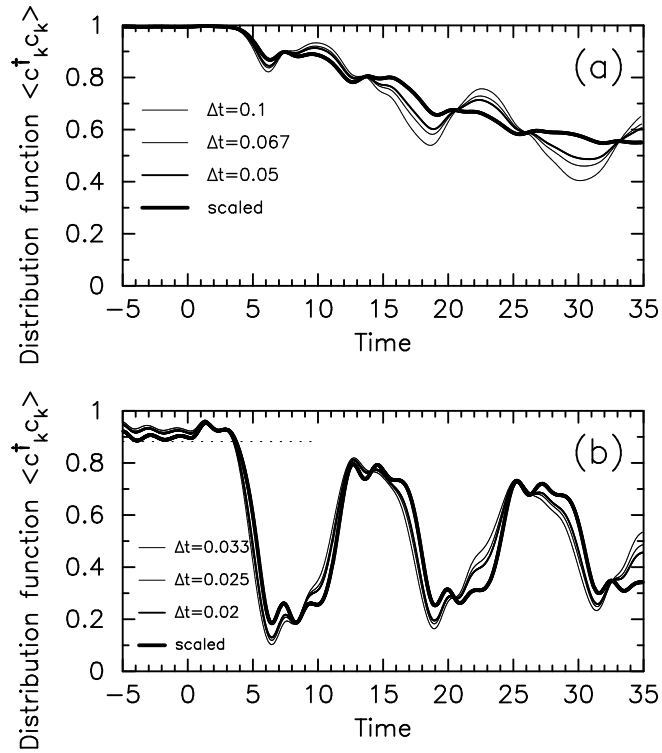


Fig. 1.8. Raw data and scaled data for the distribution function at $\epsilon_{\mathbf{k}} = -2$ and $\bar{\epsilon}_{\mathbf{k}} = -2$ for (a) $U = 0.5$ and (b) $U = 2$. Both data sets are scaled with a quadratic Lagrange extrapolation. In panel (b), the dotted line is the equilibrium distribution function (the initial temperature is $1/\beta = 0.1$). The electric field has a magnitude of 0.5, and is turned on at time $t = 0$.

calculate the distribution function by examining the *ratio* of the lesser Green's function to the retarded Green's function, which turns out to be much more accurate than examining the lesser Green's function directly. When we scale our results, it is the ratio that is scaled to the zero discretization size limit.

In Fig. 1.8, we plot the distribution function at $\epsilon = \bar{\epsilon} = -2$ for different values of the discretization size of the Kadanoff-Baym-Keldysh contour (panel a is for a metal with $U = 0.5$ and panel b is for an insulator with $U = 2$). Also included in that figure are scaled results, which are extrapolated using a quadratic Lagrange interpolation formula. One can see that in the metal, the extrapolation tends to reduce the oscillations, while in the insulator, the extrapolation is less severe of a change from the raw data with a finite discretization. In both cases we start at $1/\beta = 0.1$ and turn on a field in the diagonal direction with a magnitude of $E = 0.5$ for each Cartesian component at $t = 0$. Hence the curves should be completely flat, and agree with the

results in Fig. 1.7. This is true for the metal, and can be seen to work fairly well for the insulator (there is an oscillation of magnitude a few percent for the insulator). One surprising result is that the distribution function has much larger amplitude oscillations in the insulator than it has in the metal (when the field is on).

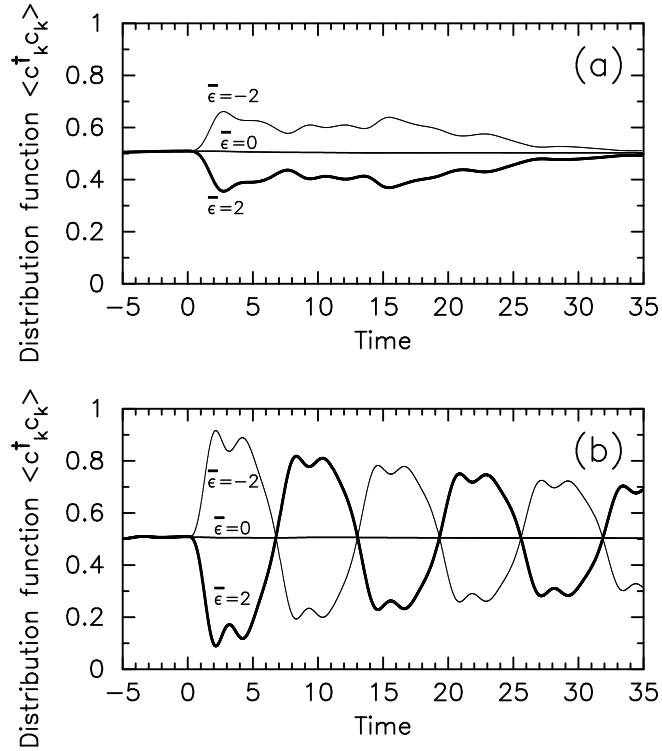


Fig. 1.9. Scaled data for the distribution function at $\epsilon_{\mathbf{k}} = 0$ and $\bar{\epsilon}_{\mathbf{k}} = -2, 0$, and 2 for (a) $U = 0.5$ and (b) $U = 2$. Both data sets are scaled with a quadratic Lagrange extrapolation. The initial temperature is $1/\beta = 0.1$; the electric field has a magnitude of 0.5 , and is turned on at time $t = 0$. Note the larger amplitude oscillations for the Mott insulator (panel b) than the metal (panel a).

Having shown that we can achieve good accuracy by scaling our results, we next focus on the $\bar{\epsilon}$ dependence of the distribution function. In Fig. 1.9, we show results for $\epsilon = 0$ and various $\bar{\epsilon}$ in the (a) metal and (b) insulator. Once again one can see much larger amplitude oscillations in the insulator, and one can see the effect of particle-hole symmetry where results for negative $\bar{\epsilon}$ values are mirror reflected from the positive ones. Note further that the oscillations seen in the equilibrium region ($t < 0$) in the previous figure are

much reduced here. The nonequilibrium oscillations are expected on general grounds as the system generically has an oscillating current develop for short times after the field is turned on. Since the oscillating current arises from (quasi)periodic changes of the electron distribution through the Brillouin zone, such oscillations in the distribution functions are consistent with an oscillating current.

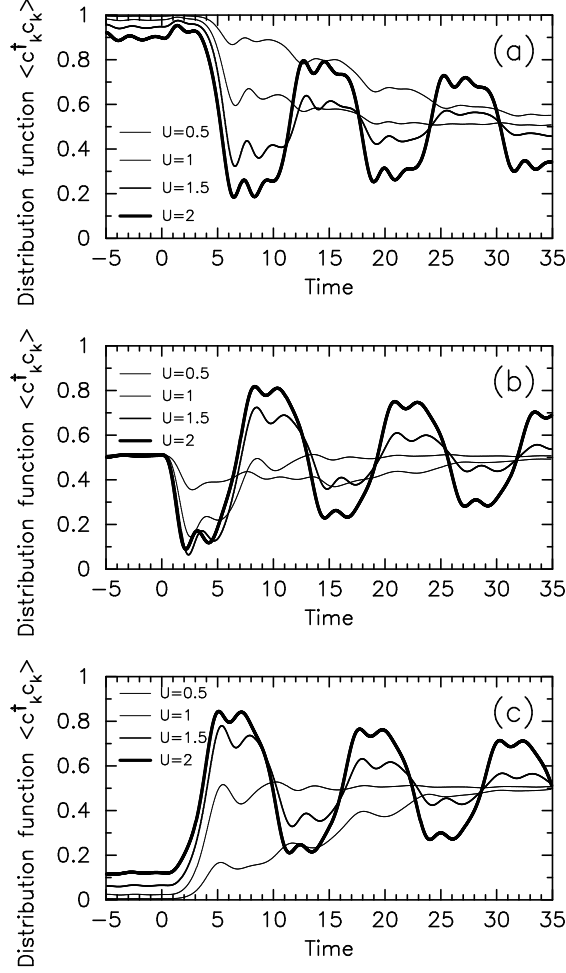


Fig. 1.10. Scaled data for the distribution functions for different U values. Panel (a) is $\epsilon_{\mathbf{k}} = -2$ and $\bar{\epsilon}_{\mathbf{k}} = -2$, panel (b) is $\epsilon_{\mathbf{k}} = 0$ and $\bar{\epsilon}_{\mathbf{k}} = 2$, and panel (c) is $\epsilon_{\mathbf{k}} = 2$ and $\bar{\epsilon}_{\mathbf{k}} = 0$.

Next, we show scaled results for specific points in the Brillouin zone with different values of U to see how the system evolves from a metal to an insulator. The most striking behavior is that the amplitude of the oscillations grow rather dramatically as the scattering increases. They are not simple sinusoidal oscillations, having complex structure to them. One can also see, by comparing with the equilibrium results for negative times, that the accuracy is quite good too (the curves are essentially flat for negative times).

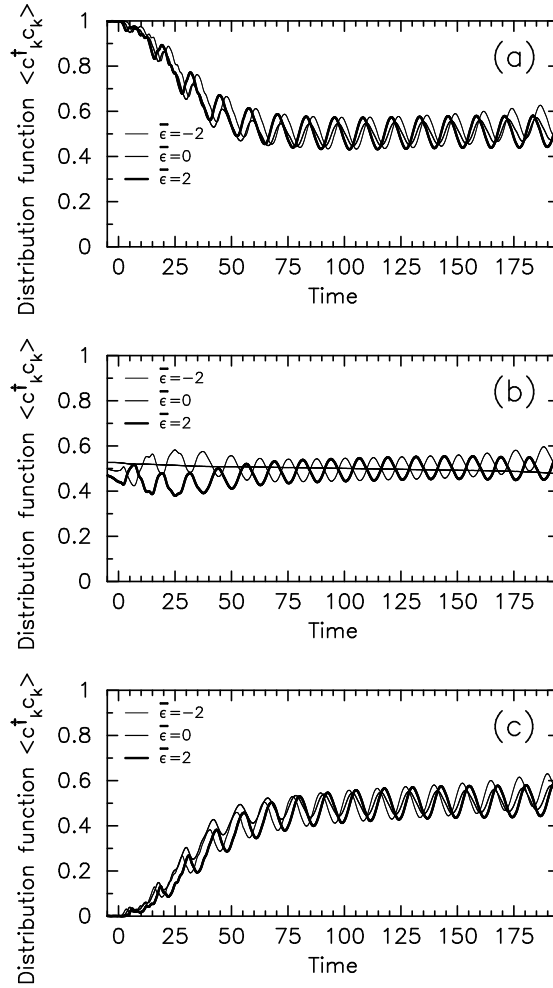


Fig. 1.11. $\Delta t = 0.1$ (unscaled) data for the distribution functions for $U = 0.25$ extended to much longer times. Panel (a) is $\epsilon_{\mathbf{k}} = -2$ and $\bar{\epsilon}_{\mathbf{k}} = -2, 0,$ and 2 ; panel (b) is $\epsilon_{\mathbf{k}} = 0$ and $\bar{\epsilon}_{\mathbf{k}} = -2, 0,$ and 2 ; and panel (c) is $\epsilon_{\mathbf{k}} = 2$ and $\bar{\epsilon}_{\mathbf{k}} = -2, 0,$ and 2 .

Finally, we show plots for the different distribution functions we have been examining for the case of weak coupling $U = 0.25$ and large times in Fig. 1.11. The data is not scaled, but rather is calculated with a fixed discretization $\Delta t = 0.1$. This could have the tendency to slightly overestimate the magnitude of the oscillations, as we have seen with our previous data. Note how in all cases except for $\epsilon = \bar{\epsilon} = 0$ we have long-lived oscillations that develop with what appears to be a well defined phase difference for different $\bar{\epsilon}$ values. The period of the oscillations is essentially the Bloch period (equal to 4π in this case).

We now consider the lesser Green's function sum rules for the Falicov-Kimball model in a field [White1991, Turkowski and Freericks2006]. The distribution functions are always equal to the occupation of the conduction electrons over the Brillouin zone. Unfortunately, unlike the retarded Green's functions, where the equal time limit is equal to one, here we do not know *a priori* what the occupations are, so we cannot use the sum rules to verify the accuracy of the calculations. The only test we can perform is to see that the results are constant for negative times and that the constant value is equal to the value calculated in an independent equilibrium formalism. Here we find the accuracy of the scaled results is pretty good for these values, with errors on the order of a few percent. Since we generically find the time formalism is less accurate for the equilibrium results than the nonequilibrium ones, we anticipate that the scaled results for the nonequilibrium distribution functions have errors that are also in the few percent range.

1.4 Conclusions

In this work, we have illustrated how dynamical mean-field theory can be generalized to nonequilibrium and applied the formalism to the spinless Falicov-Kimball model in a large electric field. We showed results for the local DOS, which plot the distribution of quantum-mechanical states, and for the distribution functions, which plot how the electrons occupy those quantum states in the Brillouin zone. Our main focus was on showing how one can scale the results to the zero discretization size limit, and how the scaled results have high accuracy. For the DOS, we compared a transient formalism to a steady-state formalism and found good agreement at long times. The distribution functions also show interesting behavior—they develop oscillations which tend to grow in amplitude as the system becomes more strongly correlated and passes from a metal to an insulator across the Mott transition. In the future, we will further investigate these distribution functions by examining their behavior through the entire Brillouin zone, rather than at just a few selected points.

Acknowledgements

This work was supported by the National Science Foundation under grant number DMR-0705266 and by DARPA under grant number W911NF-07-1-

0576. Supercomputer time was provided by the NASA NLCS program and the HPCMP of the DOD including two CAP phase II projects (one at ERDC and one at ARSC). The author also acknowledges the hospitality of NIST's Gaithersburg campus, where this work was completed. Finally, useful discussions and collaborations with A. Hewson, V. Turkowski and V. Zlatić are acknowledged.

References

- [Bertoncini and Jauho1991] Bertoncini, R. and Jauho, A. P. (1991) Gauge-invariant formulation of the intercollisional field effect including collisional broadening, *Phys. Rev. B* **44**, 3655–3664.
- [Brandt and Mielsch1989] Brandt, U. and Mielsch, C. (1989) Thermodynamics and correlation functions of the Falicov-Kimball model in large dimensions, *Z. Phys. B-Condens. Mat.* **75**, 365–370.
- [Falicov and Kimball1969] Falicov, L. M. and Kimball, J. C. (1969) Simple model for semiconductor-metal transitions: SmB_6 and transition-metal oxides, *Phys. Rev. Lett.* **22**, 997–999.
- [Freericks2007] Freericks, J. K. (2007) Transient response of strongly correlated materials to large electric fields: Utilizing the large memory capacity of ARSC's Midnight machine in a capability applications project, In D. E. Post (ed.), *Proceedings of the HPCMP Users Group Conference 2007, Pittsburgh, PA, June 18–21, 2007*, Los Alamitos, CA, p. to appear, IEEE Computer Society.
- [Freericks et al.2007] Freericks, J. K., Chang, Y.-T., and Chang, J. (2007) Demonstration of efficiency over 65% of the theoretical peak for the simulation of driven Mott insulators on the 2032 processors of the NASA Columbia supercomputer with fully portable code, *Int. J. High Perf. Comp. Appl.* p. submitted.
- [Freericks et al.2006a] Freericks, J. K., Turkowski, V. M., and Zlatić, V. (2006)a Nonequilibrium dynamical mean-field theory, *Phys. Rev. Lett.* **97**, 266408–1–4.
- [Freericks et al.2006b] Freericks, J. K., Turkowski, V. M., and Zlatić, V. (2006)b Nonlinear response of strongly correlated materials to large electric fields, In D. E. Post (ed.), *Proceedings of the HPCMP Users Group Conference 2006, Denver, CO, June 26–29, 2006*, Los Alamitos, CA, pp. 218–226, IEEE Computer Society.
- [Georges et al.1996] Georges, A., Kotliar, G., Krauth, W., and Rozenberg, M. J. (1996) Dynamical mean-field theory of strongly correlated fermion systems and the limit of infinite dimensions, *Rev. Mod. Phys.* **68**, 13–125.
- [Jauho and Wilkins1984] Jauho, A. P. and Wilkins, J. W. (1984) Theory of high-electric-field quantum transport in electron-resonant impurity systems, *Phys. Rev. B* **29**, 1919–1938.
- [Kadanoff and Baym1962] Kadanoff, L. P. and Baym, G. (1962) *Quantum Statistical Mechanics*, New York, W. A. Benjamin, Inc.
- [Keldysh1964] Keldysh, L. V. (1964) Diagram technique for nonequilibrium processes, *J. Exptl. Theoret. Phys.* **47**, 1515–1527.
- [Metzner and Vollhardt1989] Metzner, W. and Vollhardt, D. (1989) Correlated lattice fermions in $d = \infty$ dimensions, *Phys. Rev. Lett.* **62**, 324–327.
- [Peierls1933] Peierls, R. E. (1933) Theory of diamagnetism of conduction electrons, *Z. Phys.* **80**, 763–791.

- [Turkowsky and Freericks2005] Turkowski, V. M. and Freericks, J. K. (2005) Non-linear response of Bloch electrons in infinite dimensions, *Phys. Rev. B* **71**, 085104–1–11.
- [Turkowsky and Freericks2006] Turkowski, V. M. and Freericks, J. K. (2006) Spectral moment sum rules for strongly correlated electrons in time-dependent electric fields, *Phys. Rev. B* **73**, 075108–1–15.
- [Turkowsky and Freericks2007] Turkowski, V. M. and Freericks, J. K. (2007) Nonequilibrium dynamical mean-field theory of strongly correlated electrons, In J. M. P. Carmelo, J. M. B. L. dos Santos, V. R. Vieira, and P. D. Sacramento (eds.), *Strongly Correlated Systems: Coherence and Entanglement*, Singapore, pp. 187–210, World Scientific.
- [van Dongen1992] van Dongen, P. G. (1992) Exact mean-field theory of the extended simplified Hubbard model, *Phys. Rev. B* **45**, 2267–2281.
- [Wagner1991] Wagner, M. (1991) Expansions of nonequilibrium Greens functions, *Phys. Rev. B* **44**, 6104–6117.
- [White1991] White, S. R. (1991) Spectral weight function for the two-dimensional Hubbard model, *Phys. Rev. B* **44**, 4670–4673.